Atmospheric Environment 212 (2019) 142–152

Contents lists available at ScienceDirect

Atmospheric Environment

journal homepage: www.elsevier.com/locate/atmosenv

Analysis of particulate distributed across Fukushima Prefecture: Attributing provenance to the 2011 Fukushima Daiichi Nuclear Power Plant accident or an alternate emission source

Peter George Martin[a,*], Merrick Davies-Milner[b], John Nicholson[a], David Richards[c], Yosuke Yamashiki[d], Thomas Scott[a]

[a] HH Wills Physics Laboratory, Tyndall Avenue, Bristol, BS8 1TL, UK
[b] School of Earth Sciences, Wills Memorial Building, Queens Road, Bristol, BS8 1RJ, UK
[c] School of Geographical Sciences, University Road, Bristol, BS8 1SS, UK
[d] GSAIS, Kyoto University, 1 Nakaadachi-cho, Yoshida, Sakyo-ku, Kyoto, 606-8306, Japan

ARTICLE INFO

Keywords:
Fukushima
Particulate
Plume
Deposition
Uranium
REE

ABSTRACT

Over eight years have now passed since the chain of events that occurred at Japan's Fukushima Daiichi Nuclear Power Plant (FDNPP) and despite this, considerable research effort continues to be expended – yielding results pertinent to understanding the conditions behind the numerous radioactivity release events. As well as investment in this extensive scientific research, great effort is also being directed to the large-scale remediation of the radiologically-affected area and is set to continue for the foreseeable future. Central to this has been the study of the highly-volatile and high-yield fission products of cesium (^{134}Cs and ^{137}Cs) and iodine (^{129}I and ^{131}I), which were together dispersed at considerable total activities as a consequence of the accident.

In contrast to investigating the distribution (and state) of these high-activity fission products, this study examined fragments of transition metals, rare earth elements and actinides found adhered to a diverse range of organic samples collected from localities across the radiologically contaminated Fukushima Prefecture. As well as varying enormously in their elemental composition, the entrapped particulates comprised a wide size range (150 nm to > 10 μm). For particulate of certain compositions (including Ag, Ce, Sm, and Au), a correlation was observed between their size and the distance at which they were encountered from the FDNPP. While a trend was apparent for these and several other composition particles, other materials (including Zr, Pb, Sn, and Ba) could not be described by such a strongly-negative linear trend. Although a Fukushima provenance could be apportioned to a component of the material, an alternate source is necessary to account for a significant inventory of the particulate material. While contrasting provenances may exist, both the size and composition of this particulate could represent potentially significant health implications for exposed populations.

1. Introduction

The incident at the Fukushima Daiichi Nuclear Power Plant (FDNPP) was responsible for the release of a large amount of radioactive material into not just the area immediately surrounding the plant (Furuta et al., 2011; Sanada et al., 2014), but also into the neighbouring Pacific Ocean (Kawamura et al., 2011), and the wider global environment (Bolsunovsky and Dementyev, 2011; Loaiza et al., 2012; Lozano et al., 2011; Masson et al., 2011). Estimates have placed the total amount of radioactivity at between 340 PBq and 800 PBq (Chino et al., 2011; Steinhauser et al., 2014; Yasunari et al., 2011) – or 10%–15% of the total Chernobyl emission (Hamada and Ogino, 2012; Ten Hoeve and Jacobson, 2012; Winiarek et al., 2012). As a consequence of the multiple reactors involved in the accident and the widespread international ramifications it presented, the events at Fukushima were rated on the International Nuclear Event Scale (INES) at Level 7 (IAEA, 2012, 2008) – the most severe, like the Chernobyl accident and release 25 years earlier.

Elemental and isotopic analysis of material ejected from the facility has previously been performed using a diverse range of techniques – following an equally diverse range of sample preparation procedures. One of the most time and cost-efficient ways to fingerprint the gamma-emitting contamination has, and continues to be, is through gamma-ray (γ-ray) spectroscopy. Using this method, the individual gamma-ray

* Corresponding author.
E-mail address: peter.martin@bristol.ac.uk (P.G. Martin).

https://doi.org/10.1016/j.atmosenv.2019.05.043
Received 21 May 2018; Received in revised form 7 May 2019; Accepted 18 May 2019
Available online 24 May 2019

photon energies associated with decay events of the radioactive species (or their daughter products) can be measured and the results quantified, without the need for an initial lengthy, complicated and costly sample pre-preparation phase. A complementary spectroscopy method is alpha (α) particle spectroscopy. Unlike γ-spectroscopy, measuring the sub-atomic alpha-particle emissions from the nucleus of the atom to identify the emitting species (typically contaminating actinides such as U and Pu) relies on extensive sample preparation steps, a vacuum system as well as lengthy counting times to produce meaningful results for these longer-lived species (Holm and Fukai, 1977; Sill and Williams, 1981). The alternative characterisation methods of mass-spectrometry, including; inductively coupled plasma-mass spectrometry (ICP-MS) (Zheng et al., 2012), thermal ionisation mass spectrometry (TIMS) (Yuji Shibahara et al., 2014), and accelerator mass spectrometry (AMS) (Sakaguichi et al., 2012), have all been used to characterise contamination within soils and organic materials sampled from across the Fukushima-affected region. Like radionuclide spectroscopy, these spectrometry methods have near-exclusively investigated large volume (bulk) material samples (Y. Shibahara et al., 2014; Zheng et al., 2012), and not the fine-scale (individual) contaminant particulate. Comparatively few studies have been performed, focusing purely on the analysis of these individual microscopic particles (Abe et al., 2014; Adachi et al., 2013; Mukai et al., 2014; Satou et al., 2016).

Initial isolated micro-particle studies by Kaneyasu et al. (2012) (Kaneyasu et al., 2012), Tanaka et al. (2012a) (Tanaka et al., 2012b), and Kanai (2012) (Kanai, 2012) have each examined such aerosol emissions – quantifying both their particle size and radioactivity, obtained from localities surrounding the FDNPP. However, these studies focused on the volatile fission-product species emitted (e.g. Cs, I, Ag, and Te) – captured through high-volume air sampling instruments before being analysed using γ-ray spectroscopy. Having an easily detectable gamma-ray signature as well as being one of the highest-yield fission product elements (Wilson, 1996), Cs has resultantly been the primary radionuclide examined in the aftermath of the accident. While a component of the volatile radiocesium inventory has been shown to be concentrated within Si-based microparticles, resulting from the readily-volatilised nature of Cs, the majority of this radionuclide (alongside other similarly volatile species such as I, Ag, and Te) has been distributed across Fukushima Prefecture through the wet deposition of ionic species (Katata et al., 2012; Yoshida and Takahashi, 2012), rather than as the less common solid, micron-scale, particulate.

While the works of numerous studies including Kanai (2012) (Kanai, 2012), Mala et al. (2013) (Mala et al., 2013), and Masson et al. (2013) (Masson et al., 2013), have highlighted and provided some quantification of the Fukushima-derived release of particulate material into the Japanese environment; other sources of such material also exist and could be attributed to any one of a number of anthropogenic processes and industries. Extensive analysis has been performed on both trace and rare earth elements (REE) encountered in the environment at numerous sampling sites around the world; with the foremost number of studies having been conducted within Japan. Such works have investigated material encountered within soils (Yamasaki et al., 2001; Yoshida et al., 1996), incorporated within rainfall (Iwashita et al., 2011; Shimamura et al., 2007), or sampled directly as airborne particulate (Furuta et al., 2005; Suzuki et al., 2010). The enrichment of elements at concentrations above specified levels – typically normalised continental crustal abundance (Hofmann, 1988; Taylor, 1964), or the ratio of two specific elements relative to one another, are both indicators of general (or more directly attributable) anthropogenic processes. For example, the use of the La/V and La/Sm elemental ratios were invoked by Kitto et al. (1992) (Kitto et al., 1992), to represent a method for attributing such fragment material to either hydrocarbon refineries or oil-fired power plants.

In contrast to many European countries and the United States, as a result of the limited available space within Japan, the vast majority of wastes (both industrial and domestic) are incinerated at a large number of specifically-designed plants, rather than being sent directly to landfill facilities, the majority of which are located close to population centres (Sakai et al., 1996). Values placed on municipal wastes generated by the Japanese Ministry of The Environment (Japanese Ministry of the Environment, 2014), determined that 70% of all of the countries waste was incinerated, with only 20% recycled, and around 10% directed to landfill. This value is only marginally different to the 74.3% reported by Sakai et al. (1996), nearly two decades earlier. However, considerable advancements have been made in the efficiency of capturing ash otherwise released from these incineration processes, as well as the processes involved in physically combusting the waste materials (Tanaka, 1992).

An extensive number of historic works have examined and subsequently quantified particle resuspension after its initial deposition (Nicholson, 1988; Sehmel, 1980), with some studying the important influence of vehicles on remobilisation (Nicholson et al., 1989). The deposition of mineral particles (dust), prior to their resuspension, transport and secondary deposition has been viewed as important to the local heterogeneity of particle composition (Amato et al., 2013).

Through first sampling bulk material collected from a range of distances out from the FDNPP before subsequently applying high-resolution electron microscopy analysis, this work sought to investigate whether clear depositional trends existed with respect to the distribution of any matrix-contained particulate. If a correlation were observed to exist, could it be attributed solely to the Fukushima incident, natural releases, anthropogenic activity – or a combination thereof. If material could not be unequivocally attributable to Fukushima, then alternative sources are required. Due to its micron-scale dimensions, the size of the material is eminently respirable (Pope et al., 2002), and therefore poses potential health implications if it were to be inhaled.

2. Experimental

2.1. Sampling

Samples were collected from localities across Fukushima Prefecture, chosen arbitrarily to incorporate differing distances (and bearings) from the plant (Fig. 1 and Table 1) – contaminated by radiocesium to varying degrees by the accident (METI, 2015). These bulk samples were not obtained directly from the ground (e.g. grasses, roadside detritus or sediments, as in earlier studies (Mukai et al., 2014; Saito et al., 2014; Satou et al., 2016; Tanaka et al., 2012a)) but from positions above the ground where elevated levels of radioactivity were encountered – identified in each instance using a handheld Geiger counter. This organic matrix material included mosses attached to boulders, lichens adhered to trees as well as leaf-debris similarly trapped above the ground. The collection of the particulate-containing bulk samples from the various sampling sites was undertaken during trips to the contaminated Fukushima Prefecture during May 2014, May 2015 and October 2015. Although a time period between the FDNPP accident and the episodes of sample-collection from the land surrounding the sites are apparent, care was taken to ensure that the influence of other anthropogenic sources of particulate were minimised – with secluded/agricultural sites abandoned since the accident selected where the influence of roads or recent transient activity were viewed as negligible.

For collection, storage and the subsequent transportation, each gram-size sample was contained within an airtight sample pot and bagged multiple times to ensure its appropriate material/radiological containment. To safeguard against any pre-existing particulate from contaminating the results, sterilised sample pots and similarly sterilised disposable plastic tweezers were used throughout the sampling at each locality.

2.2. Sample preparation

To prepare for the examination of a small portion (typically 0.1 g) of

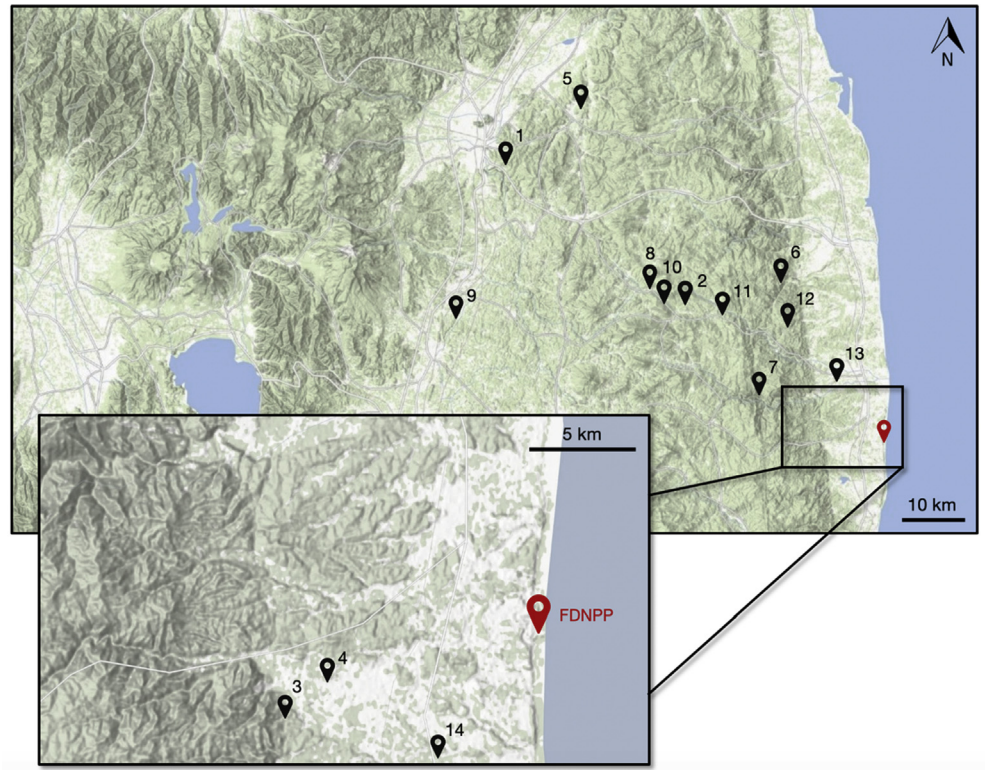

Fig. 1. Map of Fukushima Prefecture with the location of the 14 sampling sites and the coastal FDNPP identified.

Table 1
Location of the 14 sampling sites, including each sites distance from the FDNPP in addition to the bulk sample medium collected.

Site	Name (Town or City)	Latitude Longitude	Distance to FDNPP (km)[a]	Sample medium
1	Emataira (Fukushima City)	37.724482 N 140.487234 E	58.8	Leaf & Moss
2	Shimohiso (Iitate Village)	37.614174 N 140.708123 E	35.7	Lichen & Moss
3	Okuma (I) (Okuma Town)	37.400413 N 140.950743 E	6.0	Leaf & Moss
4	Okuma (II) (Okuma Town)	37.404197 N 140.971492 E	3.1	Moss
5	Kamiibuchi (Date City)	37.797488 N 140.619856 E	60.3	Leaf detritus
6	Dai (Minamisoma City)	37.604078 N 140.914587 E	22.8	Lichen & Moss
7	Katsurao (Futaba Town)	37.512471 N 140.816984 E	20.3	Moss
8	Yamakiya Junior High School (Kawamata Town)	37.602655 N 140.676441 E	37.4	Lichen & Leaf
9	Kitaosawa (Kawamata Town)	37.545626 N 140.427948 E	55.7	Lichen & Moss
10	Hirokuboyama (Kawamata Town)	37.580838 N 140.716738 E	32.9	Moss
11	Shiobite (Namie Town)	37.565656 N 140.796706 E	25.9	Moss
12	Odakaku Kanaya (Minamisoma City)	37.553426 N 140.873597 E	20.3	Moss & Lichen
13	Teramae (Namie Town)	37.491576 N 140.981855 E	8.9	Moss
14	Mukaihata (Futaba Town)	37.394940 N 141.004750 E	3.6	Moss & Lichen

[a] Direct distance measured from western site boundary.

the bulk sample, material was removed from the containing vessel before being deposited onto a low elemental background Spectro Tab (PELCO™) adhesive carbon disc. Each disc was then individually and immediately placed inside the chamber of the scanning electron microscope (SEM). The instrument was then evacuated to its standard "high-vacuum" pressure ($< 1.0 \times 10^{-5}$ mbar), where it was left for 2 h to permit for sufficient sample out-gassing to occur.

2.3. SEM and EDS

Examination of each sample was conducted within a Zeiss™ Sigma Variable Pressure (VP) Scanning Electron Microscope (S/N: 03–72, Oberkochen, Germany) with Energy Dispersive Spectroscopy (EDS) instrumentation (Octane Plus Silicon Drift Detector) and associated TEAM™ analysis software supplied by EDAX™ (Mahwah, NJ, USA). To avoid undesired contamination by sample coating (C or Au), negation of charging was achieved by utilising the Variable Pressure function of the instrument – introducing a nitrogen-rich atmosphere at comparatively low vacuum conditions (~1 mbar). A consistent working distance of 10 mm–10.5 mm, in addition to an accelerating voltage of 25 kV and 1.7 nA beam-current, were maintained throughout. To provide a rapid and accurate method of analysing large areas (mm^2), to locate points of interest, the instruments backscattered electron detector (Carl Zeiss AsB®) was used in collaboration with high-speed EDS mapping. Using the high-contrast backscatter mode, locations with high atomic (Z) number (showing as bright spots) were rapidly and automatically indexed using EDS. Points of interest were then subsequently examined with greater resolution. The smallest diameter particle identifiable was determined to be approximately 100 nm. When conducting EDS acquisition of individual particles of interest, the electron beam was rastered within a user-specified region ("free-hand area") comprising the greatest volume of the particle of interest (generally not less than 80% of the particle), with a background spectra also acquired of a substrate area immediately neighbouring the particle for comparison. A collection period of 500 s was used to maximise the signal quality. Particles of interest for future study (by mass-spectrometry, x-ray tomography or transmission electron microscopy) were physically extracted from the background matrix by in-situ micromanipulators, as described in a previous work (Martin et al., 2016).

Table 2
Average long-axis measurements (in μm) for element containing particulate observed at each of the sampling sites 1–14.

	As	Y	Zr	Ru	Pd	Ag	Cd	Sn	Sb	Te	Ba	La	Ce	Pr	Nd	Sm	Eu	Gd	Tb	Dy	Ho	Er	Yb	Hf	Ta	W	Au	Pb	Bi	Th	U	Avg.
1	–	–	1.83	–	–	0.42	–	–	–	–	–	–	1.66	–	–	–	–	–	–	–	–	–	–	–	–	–	–	–	0.84	–	1.13	1.18
2	–	–	–	–	–	1.83	2.61	0.62	–	–	0.94	–	1.34	–	–	–	–	–	–	–	–	–	–	–	–	–	0.43	0.67	–	0.27	0.58	1.03
3	–	–	–	2.65	–	3.86	–	–	–	–	0.66	–	–	–	–	–	–	–	–	–	–	–	–	–	–	–	0.98	2.08	–	–	0.94	2.62
4	–	4.31	3.19	2.94	–	3.04	–	–	–	–	0.51	–	2.74	–	–	1.35	–	–	–	–	–	–	–	–	2.03	–	1.62	2.15	1.24	–	0.47	2.55
5	–	–	3.02	–	1.43	1.16	–	–	–	–	1.88	–	1.18	–	–	0.46	–	–	0.83	0.65	–	–	–	–	0.90	–	0.60	1.37	0.63	–	–	1.26
6	–	–	1.26	1.77	–	2.12	–	2.41	–	0.61	1.21	0.63	1.50	0.77	0.59	1.27	1.63	1.31	0.82	0.76	0.80	–	0.94	–	1.21	1.07	0.95	0.91	0.70	1.08	1.64	1.16
7	–	1.16	1.59	1.52	–	1.70	–	1.88	–	–	1.07	–	1.70	1.19	1.63	–	0.74	1.11	0.72	0.95	0.94	1.47	1.35	–	0.41	–	0.74	–	1.77	1.27	0.95	1.23
8	–	–	2.46	–	–	2.51	1.96	1.56	–	–	1.35	–	1.46	–	–	–	–	–	–	–	–	–	–	2.22	–	2.28	0.70	0.77	–	–	0.70	1.56
9	–	–	0.65	–	–	0.94	–	2.83	0.53	–	2.28	1.02	0.98	0.29	–	0.40	–	0.28	0.67	0.92	0.97	1.45	–	–	–	–	0.43	–	0.86	–	0.29	0.93
10	–	–	–	1.43	–	2.86	–	3.44	0.76	2.47	1.85	–	–	1.30	–	0.84	–	0.76	1.35	–	–	–	0.98	–	–	–	0.67	2.80	0.96	1.32	2.79	1.60
11	–	–	1.27	–	–	2.22	–	–	–	–	1.12	–	1.37	–	–	–	–	–	–	–	–	–	–	–	–	–	0.86	0.72	0.83	–	1.79	1.23
12	–	–	–	1.66	–	2.51	–	1.89	2.22	–	–	–	–	–	–	–	0.87	–	–	–	–	–	–	–	3.55	–	0.72	0.89	–	3.21	0.76	1.83
13	1.52	–	–	2.18	–	3.04	–	0.75	–	–	1.22	–	–	–	–	–	–	–	–	–	–	–	–	–	–	–	1.19	1.69	1.64	–	1.54	1.66
14	–	3.53	2.34	2.82	–	2.96	–	–	–	–	0.83	–	3.26	–	–	1.51	–	–	–	–	–	–	–	–	2.16	–	1.43	2.27	–	–	1.67	2.62

2.4. Statistical analysis

To accurately analyse the large number of particles observed during this work, an extensive database was established into which the various sample metrics were input. Such metrics included: (i) measurements for the two perpendicular major axes of the fragment, (ii) its surface area (both of which were determined by the microscopes control software) as well as, (iii) its elemental composition, as determined through EDS quantification analysis.

3. Results & discussion

3.1. Particle composition

The occurrence (presented as the average long-axis particle measurements) of elements contained within particulate across the 14 sampling sites, is detailed in Table 2. Nearly all the particulate was characterised by only a single “heavier” element in addition to any number of lighter (namely transition) elements, including; O, S, Na, K, P, C, Si, Al, Fe, Mn, Ti, Cu, and Zn – varying in their weight percentage (wt%) proportions. While 99.1% of the 3000 particles characterised during this work consisted of a single “heavier” element alongside numerous accessory (lighter) elements, a minor component (< 1% of the total inventory) contained a second (or in a very small number of instances, a third) of these “heavier” elements. This bi-constituent particulate consisted only of a number of particles containing Ce and La ± Nd. Exemplar electron microscope images of typical REE-containing particles (Eu, Ho, Er and Gd) are shown in Fig. 2, alongside their associated EDS spectra. The accompanying Fig. 3 displays the average elemental composition associated with a subset of the REE-containing particles (Eu, Ho, Er, and Gd) identified within the bulk material during this study. As is shown by this plot, the wt% component of the various REEs alongside the associated accessory/transition elements that constitute the particulate vary considerably – although each particle comprises elevated components of O, Al and Si. Further apparent from Fig. 3 is the difference in the average REE wt% component per-particle – with Eu comprising the lowest average wt% (3.8 wt%) and Er the greatest (50.2 wt%). Although not occurring at concentrations within the particulate as high as O, Si and Al, the commonly observed co-existing (counter) ions of P and S occur with average concentrations within the REE-containing particulate of between 3% and 5% respectively. While some particle compositions could be aligned to naturally-occurring mineral sources (Deer et al., 2013; WebMineral, 2017), the high (> 50 wt%) concentration of Er evidenced as part of the subset of particulate presented within Fig. 3 does not align with any known mineral species. The varying proportions of all REEs (alongside other transition and actinide elements) for all particulate examined during this study is shown graphically within Fig. 4.

A plot detailing the minimum, maximum and average wt% contributions of these “heavier” elements from the entire inventory of particulate material is shown by the black lines in Fig. 4 (top). Apparent from this plot is the wide variability in these values. For example, the Ag component in particles examined in this study ranged from 5.5 wt% to 92.8 wt%, with the concentration range of both Ce and U shown to be similarly large, at 66.3 wt% and 63.9 wt% respectively. Smaller compositional ranges, however, were observed for species including As, Sb, Te and Th. Alongside the elemental abundance concentrations of the particles, the wt% compositional range of these elements when contained in naturally-occurring minerals (WebMineral, 2017), is additionally shown in Fig. 4 (by the green boxes). For many elements, the range of mineral compositions encompasses all of that element-containing particulate analysed in this work; with the abundances of Zr, Re and Te for example, all bound by these known mineral compositions. However, the wt% elemental contribution of some of the particles plots considerably outside of the compositional bounds defined by such known mineral species (WebMineral, 2017). As shown in Fig. 4, many

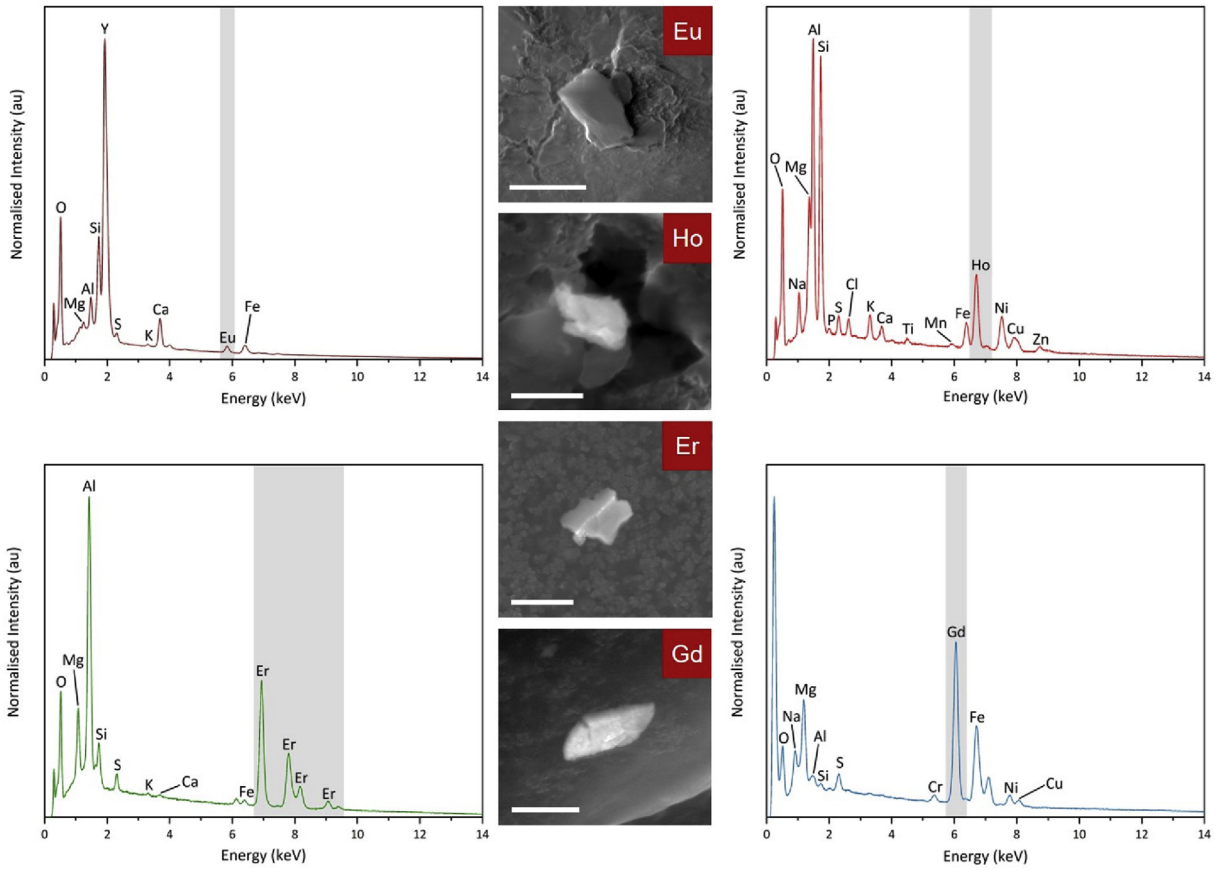

Fig. 2. Electron microscope images of exemplar particulate (Eu, Ho, Er and Gd) identified within the bulk material, alongside their corresponding EDS spectra with characteristic peaks identified.

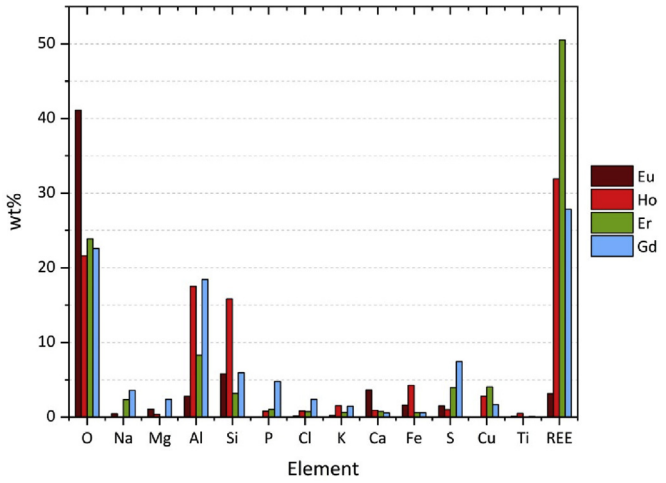

Fig. 3. Average compositional variance (as wt%) exhibited by a subset of the REE-containing particulate (Eu, Ho, Er and Gd).

of the REEs (Sm to Yb) exist in the particulate at abundances greater than maximum mineral-contained concentrations. Environmentally-sourced particles of Tb, for example, were observed to contain between 8.22 wt% and 63.66 wt% of the element (mean 31.26 wt%), while its observed mineral abundance ranges only between 0.03 wt% and 0.57 wt%. This elevated and un-natural abundance serves as strong evidence that Tb (and other composition particulate as shown in Fig. 4), is not of mineralogical origin, but rather anthropogenically-derived. It is noted that while the literature values are specified for bulk mineral crystals, potentially higher elemental concentrations/variations may be associated with/across submicron or nanometer length scales, however as was discussed formerly, the elemental quantifications associated with this work are derived from the entire particles volume and therefore represent the averaging of any intra-particle compositional variation.

The weathering/erosion followed by the environmental mobilisation and subsequent deposition of naturally-occurring mineral species is the primary means through which micron-scale material could exist adhered to bulk surfaces (Amato et al., 2013; Sehmel, 1980). This mechanism could therefore account for a proportion of the particulate material, including those containing Ag, Ba, Au and U – together observed across the majority of the sample sites. However, this natural input of material is unable to account for many of the REEs, including Gd, Ho and Er – hence, an additional mechanism is necessary to account for the existence (and resulting distribution) of this composition material.

Shown also in Fig. 4 (bottom), is the size distribution (minimum, maximum and mean average) of particulate containing each of the "heavier" elements. From this plot, a large particle size (diameter) distribution is observed (discussed subsequently below), however, it should be noted that the diameter of the REEs is on average smaller than particulate containing other, "heavier", elements – which exhibit a much larger size range and average particle diameter. The micron-scale size of a component of this particulate material will detrimentally influence the compositional results as determined via EDS elemental analysis. Owing to the sampling (interaction) volume of EDS (at 20 kV) used in this study being approximately 2 μm (Goldstein et al., 1992), characteristic x-rays will be not only generated from the particle of interest but also from the underling carbon-based mount (Spectro Tab) as well as any underling sediment/organic matrix that the particle also may be coincidentally attached to. This background signal contribution

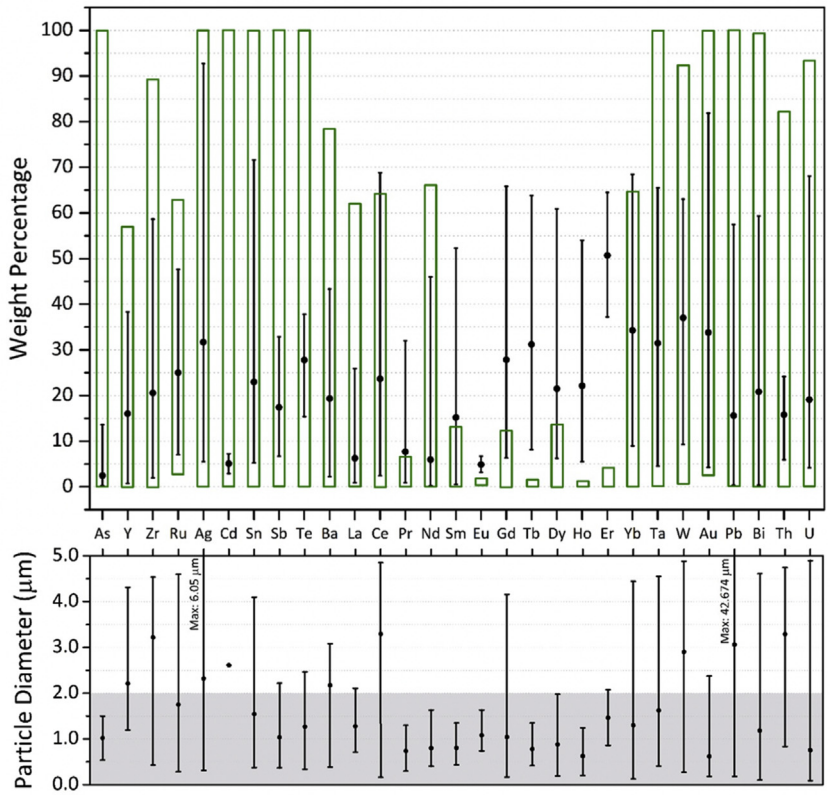

Fig. 4. *(top)* Elemental wt% composition (minimum, maximum, and mean average) of particulate across all sampling sites (black bars), alongside the wt% compositional range (green boxes) of the same elements when contained within known mineral species (WebMineral, 2017). *(bottom)* Plot detailing the observed size range (minimum, maximum and mean average) of particulate of the differing compositions identified during this study. (For interpretation of the references to colour in this figure legend, the reader is referred to the Web version of this article.)

will serve to significantly reduce (dilute) the signal intensity generated by the particle, therefore depressing the observed wt% abundances of its constituent elements. As a result, the wt% values determined in Fig. 4, for particulate with a diameter of less than 2 µm, represents an underestimation of its true composition.

Shown in Fig. 5 is a plot depicting the distribution of particle shape (roundness) – described as a measure of the particulates increasing roundness, away from that of a perfect cube. This classification is based upon the Powers Scale of Roundness (M. C. Powers, 1953), a methodology originally-devised through which to describe the shape of clasts within a sedimentary rock. Although largely qualitative, the methodology is widely-accepted – with a value of 1 denoting a particle with the highest degree of angularity, and 10 conversely ascribed to particulate with the highest level of roundness.

From these results, a skewed bi-modal distribution is observed; with the majority (c. 80%) of the particulate exhibiting a sub-rounded to rounded form (6–9), and a smaller proportion (< 15%) showing a considerably more angular particulate shape (1–3). This observed distribution, away from an angular/cuboidal crystal shape, can therefore be invoked to represent either; (i) the non-mineral origin of the particulate (owing to the mineral crystals being angular/cuboidal in form) and of resultant anthropogenic origin, or, (ii) being of natural (mineral) origin and having subsequently undergone significant transportation and weathering to yield such non-angular particulate from a previously highly-angular form.

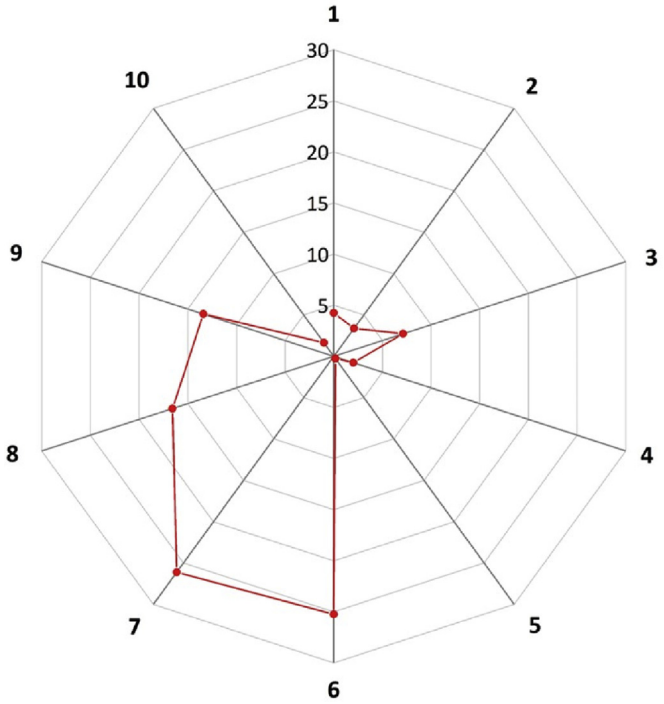

Fig. 5. Observed particulate roundness indices (as percentage of total) for all composition material, ranging from 1 (very angular/cuboidal) to 10 (well-rounded). Based on Powers (1953) (M. C. Powers, 1953).

3.2. Particle size average

A plot, independent of the materials composition, illustrating the average particle diameter for all particulate across all sampling localities, is presented in Fig. 6. While a considerable spread is observed, apparent from this plot is the small range shown by the average values (plotted in blue) of less than 3 µm – with a mean value for all material of 1.61 µm. When the vertical (particle diameter) axis is plotted logarithmically (as in Fig. 6), the trend within the data shows a linear relationship, with the mean particle diameter shown to be progressively decreasing with increasing distance away from the boundary of the FDNPP.

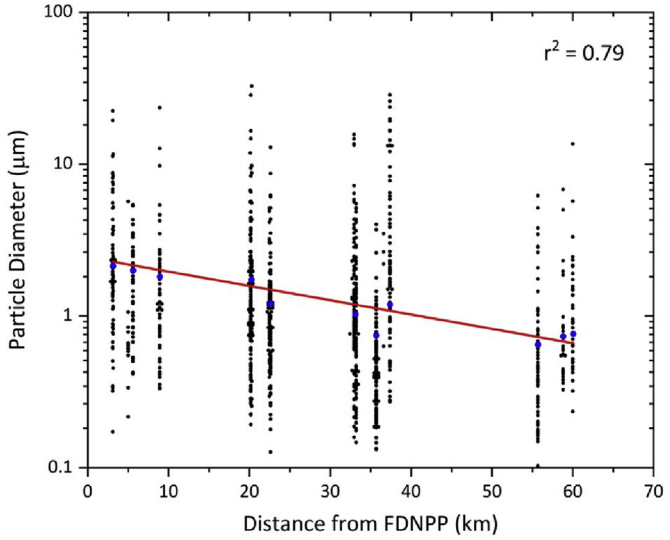

Fig. 6. Observed particle diameter reduction with increasing distance from the FDNPP, measured directly from the plant boundary to the sampling site. The average particle diameters for each sample set (distance from the FDNPP) are shown in blue, a linear trendline is applied to the data. (For interpretation of the references to colour in this figure legend, the reader is referred to the Web version of this article.)

3.3. Particle elemental size average

A linear relationship between the average particle diameter and the direct distance from the FDNPP for particulate material of specific compositions, is observed to exist. As shown in Fig. 7, for Ag, Ce, Sm, Au, Bi, and Ru, with increasing distance from the coastal reactor site, the average particle diameter is observed to decrease linearly (demonstrated by the coefficients of determination all greater than 0.71). Particulate containing Ag, whose bulk elemental and isotopic (^{110m}Ag) occurrence/concentration has formerly been quantified in earlier works (Le Petit et al., 2012; Shozugawa et al., 2012), exhibits this strongly-negative linear correlation – with particulates measured at the sites within 10 km of the plant being some of the largest encountered as part of this study (greater than or equal to 3 µm in diameter). Micron-scale particulate containing Ce, Sm, Au, and Bi all exhibit the same negative linear trend – with a marked decline in the average particle diameter with distance from the FDNPP site. Particulate of Ru composition also exhibit the same negative decline in particle size; however, particulate containing this element is observed to only exist at sampling sites located under 35 km from the FDNPP, along the primary north-westerly trending emission plume. This contrasts with the aforementioned Ag, Ce, Sm, Au and Bi containing particulate, whose existence has been identified at sites located along the entire 60 km plume length. One potential Fukushima-related release mechanism through which to explain this spatially-limited distribution results from the greater inherent density of the Ru-containing material. With a higher density than many other elements (12.1 g/cm^3) (CRC Press, 2015), such particulate would only remain "entrained" within the transporting air-mass for a limited period prior to being deposited (falling-out). Additional FDNPP associated factors that could similarly contribute to such a plant-proximal depositional trend (but require additional evaluation) result from; (i) the particulates less aerodynamic shape in comparison to the other ejecta species and/or, (ii) the Ru emission occurred during a differing (lower-energy) release phase than the other particulate material released.

Whereas Ag, Ce, Sm, Au, Bi and Ru (Fig. 7) all show a high degree of linear correlation and a tight fit to the applied negative trend-line (coefficients of determination (r^2) > 0.71), the observed distribution of U composition particulate (Fig. 8), despite depicting the same distance-related reduction in size, is not as coherent a fit as was observed for the particulate in Fig. 7 (r^2 = 0.57). Owing to the violent nature of events that occurred during March 2011 at the FDNPP; the large amounts of energy expended during the explosion would have resulted in the fragmentation of the reactor-contained U fuel.

Unlike Ag, Ce, Sm, Au, Ru and U, which are all used within or produced during the operation of a nuclear reactor, Bi is neither generated during the nuclear fission reaction (IAEA, 2017) – nor is it utilised as a reactor component or structural material (Zinkle and Was, 2013). Therefore, the negative particle size regression (with distance from the FDNPP site) likely represents such particulate having originated from a source other than the FDNPP reactors. Two additional elements used extensively within nuclear reactors globally, including those at Fukushima, are Zr and Pb. Zr (as a highly-specialist alloy, Zircaloy-4™) is used as a neutron-transparent cladding material to contain the reactors U fuel (in addition to being produced as a fission product), with Pb conversely utilised as a radiation shielding/absorbing material, and less-extensively to clad the outermost circumferences of thermally-insulated heat-exchanger pipes (Zinkle and Was, 2013). However, for materials intimately associated with nuclear reactors (produced also as nuclear fission products), neither the Zr nor Pb containing particle distribution trends mirror those of the material with compositions shown formerly in Fig. 7. As shown in Fig. 8, for Zr and Pb, no linear size reduction is apparent for these composition particulates over the 60 km extent of the plume (illustrated by the low coefficient of determination) – with both large and small material located proximally and distally from the FDNPP site. Further shown in Fig. 8, for particulate containing Sn and Ba (both fission product species with significant reactor yields (IAEA, 2017)) are particle size distributions contrasting with those formerly encountered – with particulate containing a component of either Sn and Ba showing a particle size increase (positive linear correlation) with greater distances from the coastal FDNPP. While particulate of other compositions displayed the largest diameters at sites < 10 km from the FDNPP – the inverse is observed for particulate containing both Sn and Ba.

Alongside the observed decreasing particle size trend of the Bi-containing material, and the absence of a statistical Zr and Pb distribution (despite both being used extensively/produced in nuclear reactors) – the contrasting particle size increase (with decreasing site proximity) of Sn and Ba serves to further advocate that, or a component of, such material did not result from the FDNPP accident. A plot of particulate material containing REE species average particle diameter verses distance along the plume from the FDNPP is shown in Fig. 6. Despite exhibiting a greater degree of data spread than for particulate material of other compositions, observable from this plot, however, is the marked reduction in measured diameter of this REE-containing particulate along the 60 km plume length. With an exclusively natural provenance to this particulate having been formerly excluded (Fig. 4) – an anthropogenic source-term is hence required. While various REE species are produced during the standard operation of a light water reactor (IAEA, 2017), their yields are comparatively low in comparison to other fission products, however, such REE-containing particulate have been observed with a significant abundance, as shown in Fig. 4. Consequently, a source other than the FDNPP accident is required to account for a component of this REE composition material.

It should be noted that for all composition particulate examined during this study, an element of sampling and analytical bias could detrimentally influence the results and subsequent conclusions – for example, the absence of Ru-containing material at sampling locations greater than 35 km from the FDNPP. However, through the application of automated SEM/EDS scanning for and analysis of any contained particulate from several bulk samples derived from the same sampling location, the influence of any adverse collection and analysis bias is seen as sufficiently minimised.

Combined, a more appropriate explanation for the depositional pattern of the wide range of material examined during this work arises

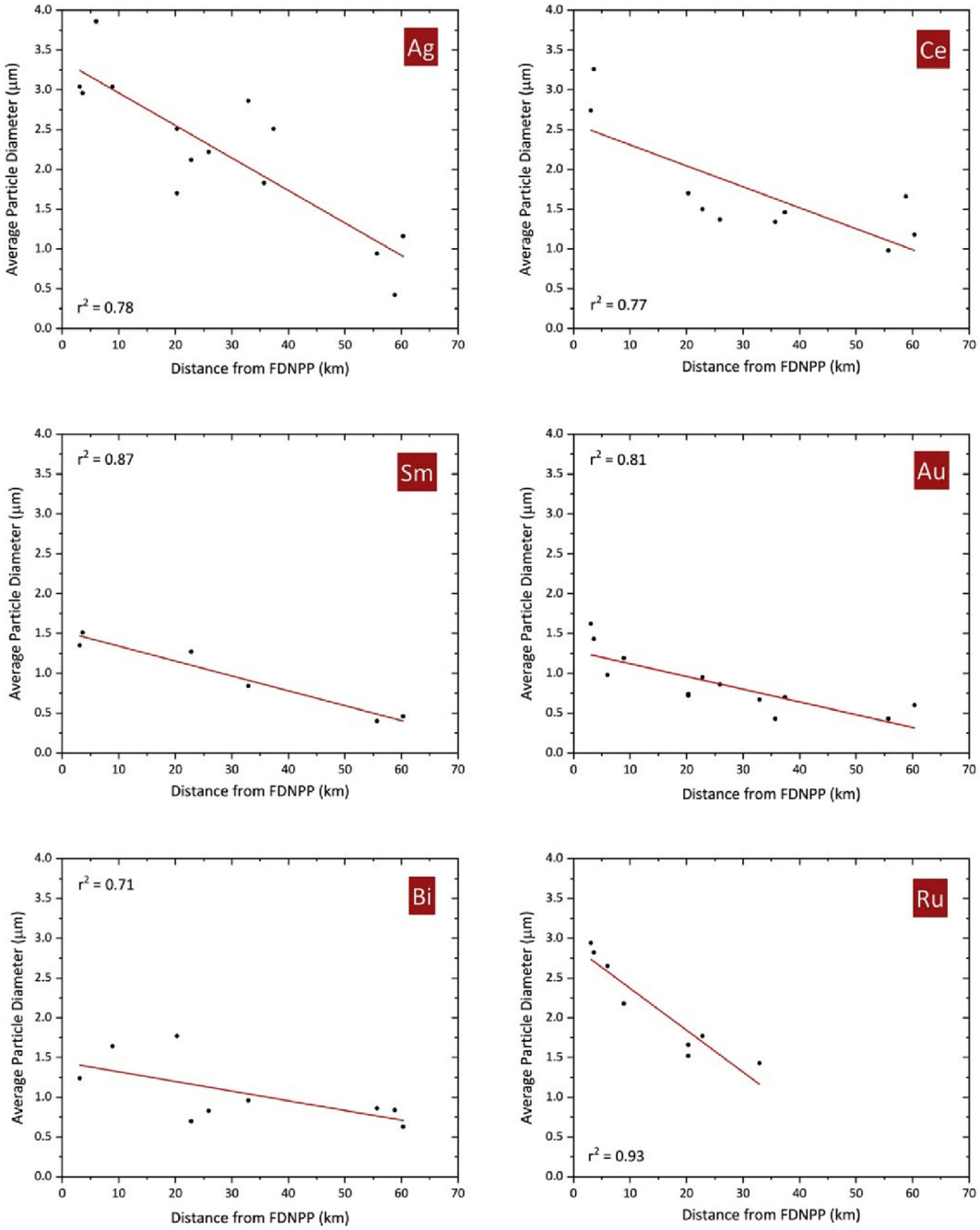

Fig. 7. Scatter plots depicting average particle diameter with distance from the FDNPP site (measured directly from the plant boundary), for elements: Ag, Ce, Sm, Au, Bi, and, Ru. The coefficient of determination (r^2 value) for each plot is shown.

from particulate contributions other than/alongside those from the FDNPP accident. To produce the spatial distribution as seen for elements Ag, Ce, Sm, Au, Bi, Ru and U – an additional emission source would have existed at a location close to the FDNPP as to yield such a decreasing size particulate with increasing distance from the coast. A contrary emission source exists for both Sn and Ba-containing material, whereby the release centre is likely located away from the FDNPP – at a position towards the furthest-more extent of the north-westerly plume. While a contribution of particulate of Zr and Pb composition may have occurred from the FDNPP, an input from an additional emission source (s) is reasonable and would serve to produce the particle size distributions shown in Fig. 6 (b) and (c). The same release source responsible for the Ag, Au, Bi, Ru and U composition material may also be responsible for the environmental contribution from the comparably-sized REE-containing material, which itself exhibits the same (reducing) depositional trend.

As formerly discussed, with waste incineration existing as the main method through which to dispose of refuge across Japan, the resulting release of micron-scale aerosol particulate (as a consequence of this process) is one mechanism to account for a component of this material. However, modern incineration and ash capture technology serves to eliminate the environmental ejection of such particulate. While various industrial production and technological manufacturing processes (alongside electronic recycling plants) all use/produce wastes of this composition, the ever-increasing value of the elements promotes their capture and recycling within developed or environmentally conscious countries. Supported by other earlier work examining analogous material deposition across mainland Japan (Sakata et al., 2014), the most-

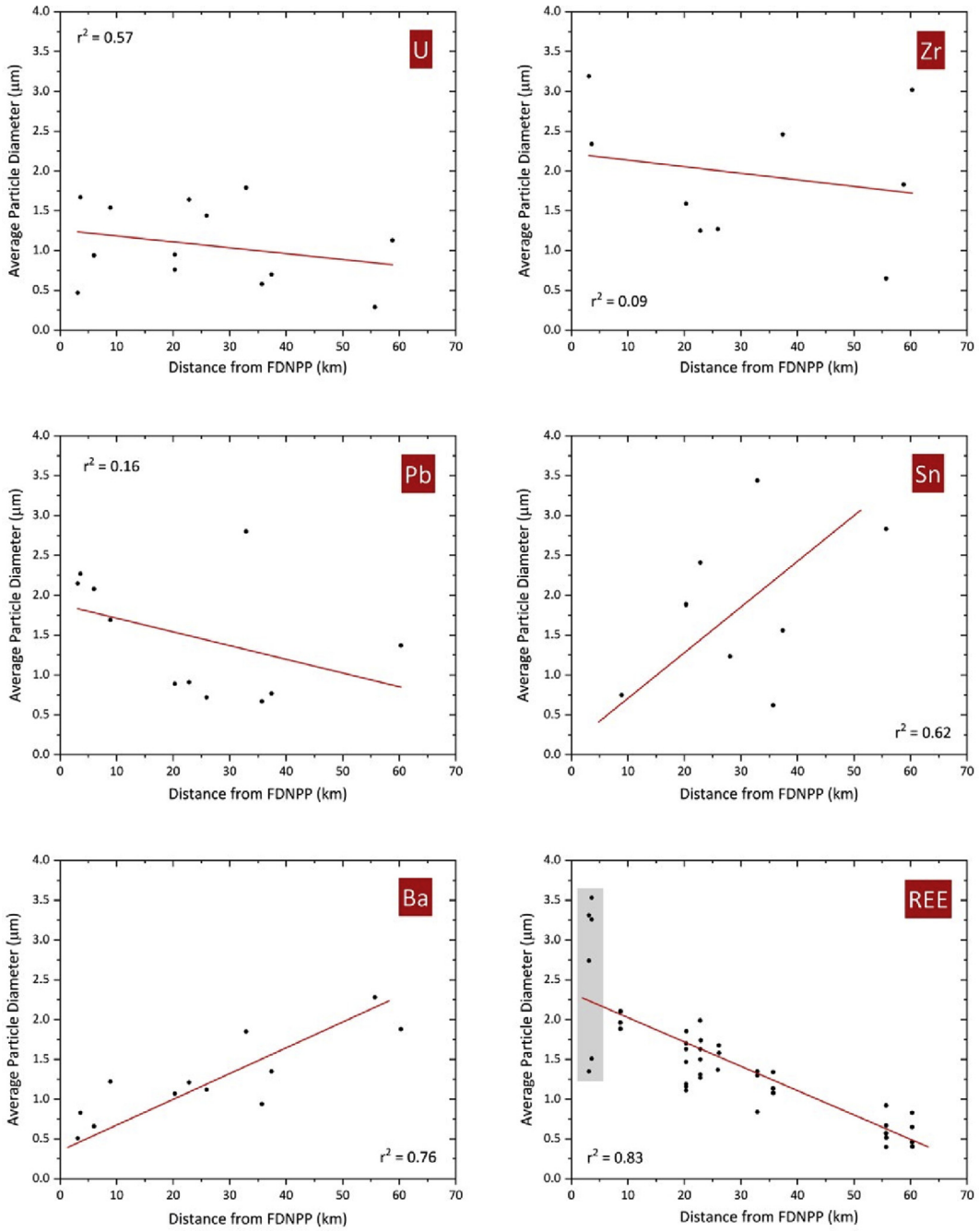

Fig. 8. Scatter plots depicting average particle diameter with distance from the FDNPP site (measured directly from the plant boundary), for elements: U, Zr, Pb, Sn, Ba, and, Rare Earth Elements (REE). The coefficient of determination (r^2 value) for each plot is shown.

probable additional source of such metal-containing particles examined during this study is the result of the long-range transportation of aerosols from other countries, in this instance mainland China (Fenger, 1999).

4. Conclusions and future work

Based on the analysis of over three thousand individual particles collected from the surfaces of plants, lichens and mosses in the region extending out from the coastal FDNPP, a considerable degree of correlation was observed to exist for material of several compositions. A mean particle size of 1.47 µm was determined for the material fragments. Whereas this study attributes the likely source of a portion of this particulate material to the March 2011 accident at the Fukushima plant, various fragment compositions cannot be as easily linked to the INES Level 7 nuclear release event.

From this work, further studies are hence required to better understand and further constrain the origin of the wide-range of fragment material identified to occur within samples obtained from within Fukushima prefecture. Such work will focus on the isolation of these individual particles of material utilising the method previously described in earlier works by the authors (Martin et al., 2016).

To attribute material unequivocally to the Fukushima accident of March 2011 and not any other emission scenarios, the key particle type of interest will be particles comprised of uranium. The identification of a non-natural ratio of $^{235}U/^{238}U$ and/or the occurrence of non-natural isotopes of the element (^{234}U and ^{236}U) will be indicative of a nuclear release scenario. Furthermore, the incorporation of additional artificial

nuclides into these particles will be a clearly defining characteristic of their in-reactor origin. For determining these ratios and the potential inclusion of further radiogenic elements, the planned work will seek to employ experimental methods such as laser ablation-inductively coupled plasma-mass spectrometry (LA-ICP-MS) and three-dimensional atom probe tomography (3D-APT), both conducted with the particulate material directly-bonded onto the fine-tipped removal needles.

In addition, the collection of further samples from the region fully-encompassing the FDNPP, would allow the existence and location of any potential additional source(s) to be identified.

As current plans to resettle large numbers of Japanese citizens originally displaced from their homes draws ever-closer, the need to understand the distribution of release material stemming from the accident is becoming increasingly important. While much of the material encountered within the environment during this study may not be the result of the FDNPP accident, as some of this material can be classified as either toxic, or has been identified to present health implications, attributing it to an emission source is equally important to both public health and wellbeing (Centers for Disease Control and Prevention, 2018; Emsley, 2003; Timbrell, 1999). Due to the micro-scale size of the material, it can be classified as easily inhalable – posing issues with regards to its respiratory uptake (Pope et al., 2002), care must hence be taken to ensure this material is not mobilised because of remedial processes that may occur.

Conflicts of interest

The authors declare no competing interests.

Acknowledgements

The authors wish to thank the citizens and local officials of Fukushima Prefecture who provided access/assisted with sampling at the numerous sites examined as part of this study. The electron microscope used in this project was funded by the UK EPSRC (Reference: EP/K040340/1), with fieldwork in Japan generously supported by the Daiwa Anglo-Japanese Foundation (Reference: 11424) and The Great Britain Sasakawa Foundation (Reference: 5223). The project was funded by the UK EPSRC (Reference: EP/S020659/1).

Appendix A. Supplementary data

Supplementary data to this article can be found online at https://doi.org/10.1016/j.atmosenv.2019.05.043.

References

Abe, Y., Iizawa, Y., Terada, Y., Adachi, K., Igarashi, Y., Nakai, I., 2014. Detection of uranium and chemical state analysis of individual radioactive microparticles emitted from the Fukushima nuclear accident using multiple synchrotron radiation X-ray analyses. Anal. Chem. 86, 8521–8525. https://doi.org/10.1021/ac501998d.

Adachi, K., Kajino, M., Zaizen, Y., Igarashi, Y., 2013. Emission of spherical cesium-bearing particles from an early stage of the Fukushima nuclear accident. Sci. Rep. 3, 5. https://doi.org/10.1038/srep02554.

Amato, F., Schaap, M., Denier van der Gon, H.A.C., Pandolfi, M., Alastuey, A., Keuken, M., Querol, X., 2013. Short-term variability of mineral dust, metals and carbon emission from road dust resuspension. Atmos. Environ. 74, 134–140. https://doi.org/10.1016/j.atmosenv.2013.03.037.

Bolsunovsky, A., Dementyev, D., 2011. Evidence of the radioactive fallout in the center of asia (Russia) following the fukushima nuclear accident. J. Environ. Radioact. 102, 1062–1064. https://doi.org/10.1016/j.jenvrad.2011.06.007.

Centers for Disease Control and Prevention, 2018. NIOSH Publications and Products [WWW Document]. CDC Fact Sheets. https://www.cdc.gov/niosh/pubs/default.html, Accessed date: 14 May 2018.

Chino, M., Nakayama, H., Nagai, H., Terada, H., Katata, G., Yamazawa, H., 2011. Preliminary estimation of release amounts of 131I and 137Cs accidently discharged from the Fukushima Daiichi nuclear power plant into the atmosphere. J. Nucl. Sci. Technol. 48, 1129–1134. https://doi.org/10.3327/jnst.48.

Deer, W., Howie, R., Zussman, J., 2013. An Introduction to the Rock-Forming Minerals. Mineralogical Society of Great Britain and Ireland. https://doi.org/10.1180/DHZ.

Emsley, J., 2003. Nature's Building Blocks: an A-Z Guide to the Elements. Oxford University Press.

Fenger, J., 1999. Urban air quality. Atmos. Environ. https://doi.org/10.1016/S1352-2310(99)00290-3. https://www.sciencedirect.com/science/article/pii/S1352231099002903.

Furuta, N., Iijima, A., Kambe, A., Sakai, K., Sato, K., 2005. Concentrations, enrichment and predominant sources of Sb and other trace elements in size classified airborne particulate matter collected in Tokyo from 1995 to 2004. J. Environ. Monit. 7, 1155–1161. https://doi.org/10.1039/b513988k.

Furuta, S., Sumiya, S., Watanabe, H., Nakano, M., Imaizumi, K., Takeyasu, M., Nakada, A., Fujita, H., Mizutani, T., Morisawa, M., Kokubun, Y., Kono, T., Nagaoka, M., Yokoyama, H., Hokama, T., Isozaki, T., Nemoto, M., Hiyama, Y., Onuma, T., Kato, C., Kurachi, T., 2011. Results of the environmental radiation monitoring following the accident at the Fukushima Daiichi Nuclear Power Plant. Interim report. Ambient radiation dose rate, radioactivity concentration in the air and radioactivity concentration in the fallout. JAEA- Rev. 35, 98.

Goldstein, J.I., Newbury, D.E., Echlin, P., Joy, D.C., Romig, A.D., Lyman, C.E., Fiori, C., Lifshin, E., 1992. Scanning Electron Microscopy and X-Ray Microanalysis: A Text for Biologists, Materials Scientists, and Geologists, second ed. Plenum Press, New York.

Hamada, N., Ogino, H., 2012. Food safety regulations: what we learned from the Fukushima nuclear accident. J. Environ. Radioact. 111, 83–99. https://doi.org/10.1016/j.jenvrad.2011.08.008.

Hofmann, A.W., 1988. Chemical differentiation of the Earth: the relationship between mantle, continental crust, and oceanic crust. Earth Planet. Sci. Lett. 90, 297–314. https://doi.org/10.1016/0012-821X(88)90132-X.

Holm, E., Fukai, R., 1977. Method for multi-element alpha-spectrometry of actinides and its application to environmental radioactivity studies. Talanta 24, 659–664. https://doi.org/10.1016/0039-9140(77)80061-1.

IAEA, 2008. The International Nuclear and Radiological Event Scale User's Manual. International Atomic Energy Agency, Vienna, Austria.

IAEA, 2012. Re-evaluation of INES Rating; Effect to the Nuclear Facilities from the Earthquake on East Area of Japan, NEWS: the Information Channel on Nuclear and Radiological Events. Vienna.

IAEA, 2017. Cumulative fission yields. [WWW Document]. URL. https://www-nds.iaea.org/sgnucdat/c3.htm, Accessed date: 21 March 2017.

Iwashita, M., Saito, A., Arai, M., Furusho, Y., Shimamura, T., 2011. Determination of rare earth elements in rainwater collected in suburban Tokyo. Geochem. J. 45, 187–197. https://doi.org/10.2343/geochemj.1.0121.

Japanese Ministry of the Environment, 2014. History and Current State of Waste Management in Japan. Tokyo.

Kanai, Y., 2012. Monitoring of aerosols in tsukuba after fukushima nuclear power plant incident in 2011. J. Environ. Radioact. 111, 33–37. https://doi.org/10.1016/j.jenvrad.2011.10.011.

Kaneyasu, N., Ohashi, H., Suzuki, F., Okuda, T., Ikemori, F., 2012. Sulfate aerosol as a potential transport medium of radiocesium from the Fukushima nuclear accident. Environ. Sci. Technol. 46, 5720–5726. https://doi.org/10.1021/es204667h.

Katata, G., Terada, H., Nagai, H., Chino, M., 2012. Numerical reconstruction of high dose rate zones due to the Fukushima Dai-ichi Nuclear Power Plant accident. J. Environ. Radioact. 111, 2–12. https://doi.org/10.1016/j.jenvrad.2011.09.011.

Kawamura, H., Kobayashi, T., Furano, A., In, T., Ishikawa, Y., Nakayama, T., Shima, S., Awaji, T., 2011. Preliminary numerical experiments on oceanic dispersion of 131 I and 137 Cs discharged into the ocean because of the fukushima Daiichi nuclear power plant disaster. J. Nucl. Sci. Technol. 48, 1349–1356. https://doi.org/10.1080/18811248.2011.9711826.

Kitto, M.E., Anderson, D.L., Gordon, G.E., Olmez, I., 1992. Rare-earth distributions in catalysts and airborne particles. Environ. Sci. Technol. 26, 1368–1375. https://doi.org/10.1021/es00031a014.

Le Petit, G., Douysset, G., Ducros, G., Gross, P., Achim, P., Monfort, M., Raymond, P., Pontillon, Y., Jutier, C., Blanchard, X., Taffary, T., Moulin, C., 2012. Analysis of radionuclide releases from the fukushima dai-ichi nuclear power plant accident Part I. Pure Appl. Geophys. 171, 629–644. https://doi.org/10.1007/s00024-012-0581-6.

Loaiza, P., Brudanin, V., Piquemal, F., Reyss, J.L., Stekl, I., Warot, G., Zampaolo, M., 2012. Air radioactivity levels following the Fukushima reactor accident measured at the Laboratoire Souterrain de Modane, France. J. Environ. Radioact. 114, 66–70. https://doi.org/10.1016/j.jenvrad.2012.03.003.

Lozano, R.L., Hernández-Ceballos, M.A., Adame, J.A., Casas-Ruíz, M., Sorribas, M., Miguel, E.G.S., Bolívar, J.P., 2011. Radioactive impact of Fukushima accident on the Iberian Peninsula: evolution and plume previous pathway. Environ. Int. 37, 1259–1264. https://doi.org/10.1016/j.envint.2011.06.001.

Mala, H., Rulik, P., Beckova, V., Mihalik, J., Slezakova, M., 2013. Particle size distribution of radioactive aerosols after the Fukushima and the Chernobyl accidents. J. Environ. Radioact. 126, 92–98. https://doi.org/10.1016/j.jenvrad.2013.07.016.

Martin, P.G., Griffiths, I., Jones, C.P., Stitt, C.A., Davies-Milner, M., Mosselmans, J.F.W., Yamashiki, Y., Richards, D.A., Scott, T.B., 2016. In-situ removal and characterisation of uranium-containing particles from sediments surrounding the Fukushima Daiichi Nuclear Power Plant. Spectrochim. Acta Part B At. Spectrosc. 117, 1–7. https://doi.org/10.1016/j.sab.2015.12.010.

Masson, O., Baeza, A., Bieringer, J., Brudecki, K., Bucci, S., Cappai, M., Carvalho, F.P., Connan, O., Cosma, C., Dalheimer, A., Didier, D., Depuydt, G., De Geer, L.E., De Vismes, A., Gini, L., Groppi, F., Gudnason, K., Gurriaran, R., Hainz, D., Halldorsson, O., Hammond, D., Hanley, O., Holey, K., Homoki, Z., Ioannidou, A., Isajenko, K., Jankovic, M., Katzlberger, C., Kettunen, M., Kierepko, R., Kontro, R., Kwakman, P.J.M., Lecomte, M., Leon Vintro, L., Leppanen, A.-P., Lind, B., Lujaniene, G., Mc Ginnity, P., Mc Mahon, C., Mala, H., Manenti, S., Manolopoulou, M., Mattila, A., Mauring, A., Mietelski, J.W., Moller, B., Nielsen, S.P., Nikolic, J., Overwater, R.M.W., Palsson, S.E., Papastefanou, C., Penev, I., Pham, M.K., Povinec, P.P., Rameback, H., Reis, M.C., Ringer, W., Rodriguez, A., Rulik, P., Saey, P.R.J., Samsonov, V., Schlosser,

C., Sgorbati, G., Silobritiene, B.V., Soderstrom, C., Sogni, R., Solier, L., Sonck, M., Steinhauser, G., Steinkopff, T., Steinmann, P., Stoulos, S., Sykora, I., Todorovic, D., Tooloutalaie, N., Tositti, L., Tschiersch, J., Ugron, A., Vagena, E., Vargas, A., Wershofen, H., Zhukova, O., 2011. Tracking of airborne radionuclides from the damaged Fukushima Dai-ichi nuclear reactors by European networks. Environ. Sci. Technol. 45, 7670–7677. https://doi.org/10.1021/es2017158.

Masson, O., Ringer, W., Mala, H., Rulik, P., Dlugosz-Lisiecka, M., Eleftheriadis, K., Meisenberg, O., De Vismes-Ott, A., Gensdarmes, F., 2013. Size distributions of airborne radionuclides from the fukushima nuclear accident at several places in europe. Environ. Sci. Technol. 47, 10995–11003. https://doi.org/10.1021/es401973c.

METI, 2015. Areas to which Evacuation Orders have been issued. [WWW Document]. URL. http://www.meti.go.jp/english/earthquake/nuclear/roadmap/pdf/150905MapOfAreas.pdf, Accessed date: 13 May 2016.

Mukai, H., Hatta, T., Kitazawa, H., Yamada, H., Yaita, T., Kogure, T., 2014. Speciation of radioactive soil particles in the Fukushima contaminated area by IP autoradiography and microanalyses. Environ. Sci. Technol. 48, 13053–13059. https://doi.org/10.1021/es502849e.

Nicholson, K.W., 1988. A review of particle resuspension. Atmos. Environ. 22, 2639–2651. https://doi.org/10.1016/0004-6981(88)90433-7.

Nicholson, K.W., Branson, J.R., Giess, P., Cannell, R.J., 1989. The effects of vehicle activity on particle resuspension. J. Aerosol Sci. 20, 1425–1428. https://doi.org/10.1016/0021-8502(89)90853-7.

Pope III, C.A., Burnett, R.T., Thun, M.J., Calle, E.E., Krewski, D., Ito, K., Thurston, G.D., 2002. Lung cancer, cardiopulmonary mortality, and long-term exposure to fine particulate air pollution. J. Am. Med. Assoc. 287, 1132–1141. https://doi.org/10.1001/jama.287.9.1132.

Powers, M.C., 1953. A new roundness scale for sedimentary particles. J. Sediment. Res. 23, 117–119. https://doi.org/10.1306/d4269567-2b26-11d7-8648000102c1865d.

Press, C.R.C., 2015. CRC Handbook of Chemistry and Physics - Summary Properties of the Elements, 96th Ed. (Boca Raton, Florida).

Saito, T., Makino, H., Tanaka, S., 2014. Geochemical and grain-size distribution of radioactive and stable cesium in Fukushima soils: implications for their long-term behavior. J. Environ. Radioact. 138, 11–18. https://doi.org/10.1016/j.jenvrad.2014.07.025.

Sakaguichi, A., Kadokura, A., Steier, P., Tanaka, K., Takahashi, Y., Chiga, H., Matsushima, A., Nakashima, S., Onda, Y., 2012. Isotopic determination of U, Pu and Cs in environmental waters following the fukushima Daiichi nuclear power plant accident. Geochem. J. 46, 355–360. https://doi.org/10.2343/geochemj.2.0216.

Sakai, S., Sawell, S.E., Chandler, A.J., Eighmy, T.T., Kosson, D.S., Vehlow, J., Van Der Sloot, H.A., Hartlén, J., Hjelmar, O., 1996. World Trends in Municipal Solid Waste Management. Waste Manag. https://doi.org/10.1016/S0956-053X(96)00106-7.

Sakata, M., Ishikawa, T., Mitsunobu, S., 2014. Contribution of Asian outflow to atmospheric concentrations of sulfate and trace elements in aerosols during winter in Japan. Geochem. J. 48, 479–490. https://doi.org/10.2343/geochemj.2.0323.

Sanada, Y., Kondo, A., Sugita, T., Nishizawa, Y., Youichi, Y., Kazutaka, I., Yasunori, S., Torii, T., 2014. Radiation monitoring using an unmanned helicopter in the evacuation zone around the Fukushima Daiichi nuclear power plant. Explor. Geophys. https://doi.org/10.1071/EG13004.

Satou, Y., Sueki, K., Sasa, K., Adachi, K., Igarashi, Y., 2016. First successful isolation of radioactive particles from soil near the Fukushima Daiichi Nuclear Power Plant. Anthropocene 14, 71–76. https://doi.org/10.1016/j.ancene.2016.05.001.

Sehmel, G.A., 1980. Particle resuspension: a review. Environ. Int. 4, 107–127. https://doi.org/10.1016/0160-4120(80)90005-7.

Shibahara, Yuji, Kubota, T., Fujii, T., Fukutani, S., Ohta, T., Takamiya, K., Okumura, R., Mizuno, S., Yamana, H., 2014a. Analysis of cesium isotope compositions in environmental samples by thermal ionization mass spectrometry - 1. A preliminary study for source analysis of radioactive contamination in Fukushima prefecture. J. Nucl. Sci. Technol. 51, 575–579. https://doi.org/10.1080/00223131.2014.891954.

Shibahara, Y., Kubota, T., Fujii, T., Fukutani, S., Ohta, T., Takamiya, K., Okumura, R., Mizuno, S., Yamana, H., 2014b. 235U/238U Isotopic ratio in plant samples from Fukushima Prefecture. J. Radioanal. Nucl. Chem. 303, 1421–1424. https://doi.org/10.1007/s10967-014-3542-y.

Shimamura, T., Iwashita, M., Iijima, S., Shintani, M., Takaku, Y., 2007. Major to ultra trace elements in rainfall collected in suburban Tokyo. Atmos. Environ. 41, 6999–7010. https://doi.org/10.1016/j.atmosenv.2007.05.010.

Shozugawa, K., Nogawa, N., Matsuo, M., 2012. Deposition of fission and activation products after the Fukushima Dai-ichi nuclear power plant accident. Environ. Pollut. 163, 243–247. https://doi.org/10.1016/j.envpol.2012.01.001.

Sill, C.W., Williams, R.L., 1981. Preparation of actinides for alpha spectrometry without electrodeposition. Anal. Chem. 53, 412–415. https://doi.org/10.1021/ac00226a008.

Steinhauser, G., Brandl, A., Johnson, T.E., 2014. Comparison of the Chernobyl and Fukushima nuclear accidents: a review of the environmental impacts. Sci. Total Environ. 470–471, 800–817. https://doi.org/10.1016/j.scitotenv.2013.10.029.

Suzuki, Y., Suzuki, T., Furuta, N., 2010. Determination of rare earth elements (REES) in airborne particulate matter (APM) collected in Tokyo, Japan, and a positive anomaly of europium and terbium. Anal. Sci. 26, 929–935. ([pii]). https://doi.org/JST.JSTAGE/analsci/26.929.

Tanaka, M., 1992. Reduction of and resource recovery from municipal solid waste in Japan. Waste Manag. Res. 10, 453–459. https://doi.org/10.1016/0734-242X(92)90119-6.

Tanaka, K., Sakaguchi, A., Kanai, Y., Tsuruta, H., Shinohara, A., Takahashi, Y., 2012a. Heterogeneous distribution of radiocesium in aerosols, soil and particulate matters emitted by the Fukushima Daiichi Nuclear Power Plant accident: retention of microscale heterogeneity during the migration of radiocesium from the air into ground and rive. J. Radioanal. Nucl. Chem. 295, 1927–1937. https://doi.org/10.1007/s10967-012-2160-9.

Tanaka, K., Takahashi, Y., Sakaguchi, A., Umeo, M., Hayakawa, S., Tanida, H., Saito, T., Kanai, Y., 2012b. Vertical profiles of iodine-131 and cesium-137 in soils in fukushima prefecture related to the fukushima Daiichi nuclear power station accident. Geochem. J. 46, 73–76. https://doi.org/10.2343/geochemj.1.0137.

Taylor, S.R., 1964. Abundance of chemical elements in the continental crust: a new table. Geochem. Cosmochim. Acta 28, 1273–1285. https://doi.org/10.1016/0016-7037(64)90129-2.

Ten Hoeve, J.E., Jacobson, M.Z., 2012. Worldwide health effects of the Fukushima Daiichi nuclear accident. Energy Environ. Sci. 5, 8743–8757. https://doi.org/10.1039/c2ee22019a.

Timbrell, J., 1999. Principles of Biochemical Toxicology, third ed. CRC Press. https://doi.org/10.1007/s13398-014-0173-7.2.

WebMineral, 2017. Minerals by Chemical Composition. [WWW Document]. URL. http://webmineral.com/chemical.shtml#.WN0y61UrJhE, Accessed date: 30 March 2017.

Wilson, P.D., 1996. The Nuclear Fuel Cycle : from Ore to Wastes. Oxford University Press, Oxford.

Winiarek, V., Bocquet, M., Saunier, O., Mathieu, A., 2012. Estimation of errors in the inverse modeling of accidental release of atmospheric pollutant: application to the reconstruction of the cesium-137 and iodine-131 source terms from the Fukushima Daiichi power plant. J. Geophys. Res. Atmos. 117, 16. https://doi.org/10.1029/2011JD016932.

Yamasaki, S., Takeda, A., Nanzyo, M., Taniyama, I., Nakai, M., 2001. Background levels of trace and ultra-trace elements in soils of Japan. Soil Sci. Plant Nutr. 47, 755–765. https://doi.org/10.1080/00380768.2001.10408440.

Yasunari, T.J., Stohl, A., Hayano, R.S., Burkhart, J.F., Eckhardt, S., Yasunari, T., 2011. Cesium-137 deposition and contamination of Japanese soils due to the Fukushima nuclear accident. Proc. Natl. Acad. Sci. U. S. A 108, 19530–19534. https://doi.org/10.1073/pnas.1112058108.

Yoshida, N., Takahashi, Y., 2012. Land-surface contamination by radionuclides from the fukushima Daiichi nuclear power plant accident. Elements 8, 201–206. https://doi.org/10.2113/gselements.8.3.201.

Yoshida, S., Muramatsu, Y., Tagami, K., Uchida, S., 1996. Determination of major and trace elements in Japanese rock reference samples by ICP-MS. Int. J. Environ. Anal. Chem. 63, 195–206. https://doi.org/10.1080/03067319608026266.

Zheng, J., Tagami, K., Watanabe, Y., Uchida, S., Aono, T., Ishii, N., Yoshida, S., Kubota, Y., Fuma, S., Ihara, S., 2012. Isotopic evidence of plutonium release into the environment from the Fukushima DNPP accident. Sci. Rep. 2, 8. https://doi.org/10.1038/srep00304.

Zinkle, S.J., Was, G.S., 2013. Materials challenges in nuclear energy. Acta Mater. 61, 735–758. https://doi.org/10.1016/j.actamat.2012.11.004.